Photochemistry and Vibrational Spectra of Matrix-Isolated Methyl 4-Chloro-5-phenylisoxazole-3-carboxylate

ARTICLE *in* THE JOURNAL OF PHYSICAL CHEMISTRY A · FEBRUARY 2011

Impact Factor: 2.69 · DOI: 10.1021/jp110705c · Source: PubMed

THE JOURNAL OF PHYSICAL CHEMISTRY A

ARTICLE

pubs.acs.org/JPCA

Photochemistry and Vibrational Spectra of Matrix-Isolated Methyl 4-Chloro-5-phenylisoxazole-3-carboxylate

Susy Lopes,[†] Cláudio M. Nunes,[†] Andrea Gómez-Zavaglia,[†,‡] Teresa M. V. D. Pinho e Melo,[†] and Rui Fausto*[,†]

[†]Department of Chemistry, University of Coimbra, P-3004-535 Coimbra, Portugal

[‡]Centro de Investigación y Desarrollo en Criotecnología de Alimentos (Conicet La Plata, UNLP), RA-1900, Argentina

Supporting Information

ABSTRACT: Methyl 4-chloro-5-phenylisoxazole-3-carboxylate (MCPIC) has been synthesized, isolated in low temperature argon and xenon matrices, and studied by FTIR spectroscopy. The characterization of the low energy conformers of MCPIC was made by undertaking a systematic investigation of the DFT(B3LYP)/6-311++G(d,p) potential energy surface of the molecule. The theoretical calculations predicted the existence of three low energy conformers. Two of them (**I** and **II**) were observed experimentally in the cryogenic matrices. The third one (**III**) was found to be converted into conformer **II** during deposition of the matrices, a result that is in agreement with the predicted low **III** → **II** energy barrier (<0.3 kJ mol^{-1}) . In situ UV irradiation (λ > 235 nm) of matrix-isolated MCPIC yielded as final photoproduct the corresponding oxazole (methyl 4-chloro-5-phenyl-1,3-oxazole-2-carboxylate). Identification of the azirine and nitrile-ylide intermediates in the spectra of the irradiated matrices confirmed their mechanistic relevance in the isoxazole → oxazole photoisomerization.

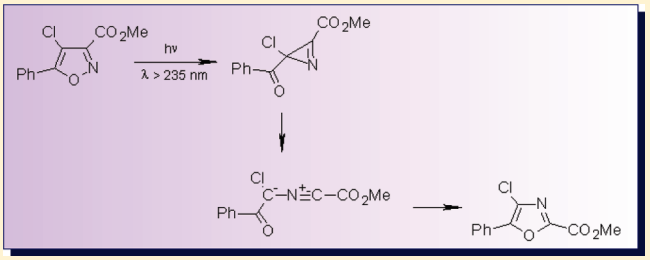

INTRODUCTION

Isoxazole and its derivatives are important building blocks of many compounds of biological interest. These heterocycles are reactants or intermediates in the synthesis of compounds that have been receiving pharmaceutical and medicinal applications.[1−12] In particular, several phenylisoxazoles with halogen or multiple halogen substituents have been reported as anthelmintics or possessing antiparasitic activity.[13,14] The agricultural uses of isoxazole derivatives include herbicidal, insecticidal, and soil fungicidal activities.[15−18] Isoxazoles have also been used as semiconductors, as corrosion inhibitors in fuels and lubrificants, and in the production of photographic and liquid crystalline materials.[19−25]

Isoxazoles (**1**, in Scheme 1), including the unsubstituted compound, have been the subject of many studies by different well-known techniques, such as infrared (IR), Raman, NMR, and microwave spectroscopies, mass spectrometry, and X-ray diffraction.[6,9,10,26−29] Many studies combined experimental techniques and theoretical methods at various levels of approximation, such as DFT and MP2.[30−34] One of the most interesting features of the reactivity of isoxazoles is their capability to be converted into other heterocyclic compounds through a ring-opening reaction and subsequent recyclization. The first step of this type of chemical transformation is the cleavage of the labile N−O single bond, which can be either thermally[35−40] or photochemically induced.[40−45] The generation of vinyl nitrene intermediates (**2**) has been proposed,[37,39−41,44] which rearrange into the corresponding 2*H*-azirines (**3**). The 2*H*-azirines can

Scheme 1

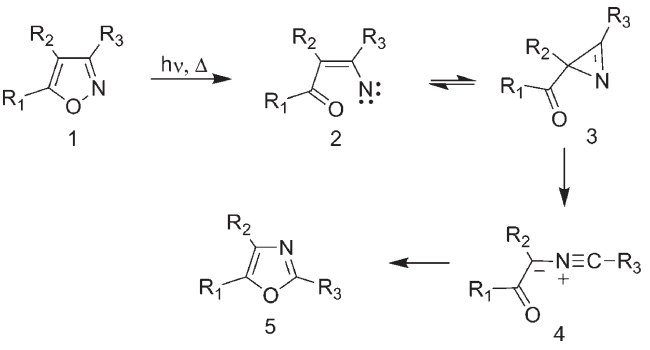

then undergo ring cleavage to nitrile-ylides (**4**) followed by recyclization to give oxazoles (**5**) as the final products (see Scheme 1).[37,38,43−45] Although the detection of the 2*H*-azirines is not always possible, their presence has been inferred in the isoxazole−oxazole rearrangement. The nature of the substituents and their position in the isoxazole ring are also important factors in determining the preferred reactive pathway and details of the chemical reactivity of isoxazoles.[46−48]

Received: November 9, 2010
Revised: January 5, 2011
Published: February 3, 2011

Chart 1

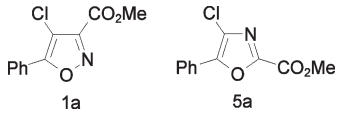

In a previous publication,[49] the monomeric forms of methyl 4-chloro-5-phenylisoxazole-3-carboxylate (MCPIC; **1a** in Chart 1) and its oxazole counterpart, methyl 4-chloro-5-phenyl-1,3-oxazole-2-carboxylate (MCPOC; **5a**) were studied using matrix-isolation infrared spectroscopy (argon matrix) and quantum chemical calculations. That study confirmed unambiguously the vibrational signature of both heterocycles through direct comparison of the experimental spectra of both compounds with the corresponding calculated spectra. The conformational space of MCPOC was subsequently investigated in detail both experimentally and theoretically,[50] the compound representing an interesting case where an inversion of the order of stability of the two most stable conformers occurs upon going from the gas phase to a xenon matrix.

In the present study, details of the vibrational spectra of matrix-isolated MPCIC (both in argon and xenon matrices) and its photochemistry were investigated using matrix-isolation infrared spectroscopy and DFT calculations. As it will be shown in detail below, the present study allowed us to conclude that, among the three low energy forms of MPCIC present in significant amount in the gas phase room temperature equilibrium, only two of them could be trapped in the matrices. On the other hand, the third conformer converts into one of the observed forms during deposition of the matrices. These results could be explained taking into account the calculated energy barriers separating the different MPCIC conformers. UV irradiation (λ > 235 nm) of matrix-isolated MCPIC led to its conversion to the corresponding oxazole, with the azirine and nitrile-ylide intermediates being experimentally detected, thus confirming the previously proposed mechanism for the isoxazole → oxazole photoisomerization.[40−45]

EXPERIMENTAL PROCEDURES

The procedure for the synthesis of MCPIC has been reported elsewhere.[49] Briefly, a solution of methyl 5-phenylisoxazole-3-carboxylate and *N*-chlorosuccinimide in 7% fuming nitric acid in acetic acid was irradiated with microwaves at 160 °C for about 40 min. After the solution was cooled to room temperature, water was added and the mixture extracted with CH_2Cl_2, and the organic phase was dried ($MgSO_4$) and evaporated off. The crude product was purified by flash chromatography [ethyl acetate−hexane (1:5)], to give MCPIC as a white solid (59%) [mp 62−63 °C; IR (KBr) 1221, 1441, 1738, 2957 cm^{-1}; ^1H NMR 4.03 (3H, s), 7.52−7.55 (3H, m), 8.03−8.06 (2H, m); ^{13}C NMR 53.1, 106.0, 125.6, 126.6, 129.0, 131.2, 153.3, 159.1, 165.8; MS (EI) *m*/*z* 237 (M^+, 99), 206 (14), 105 (100), 77 (68), 59 (78); HRMS (CI) *m*/*z* 237.0200 ($C_{11}H_8NO_3Cl$ [M^+], 237.0193).

Matrices were prepared by codeposition of MCPIC vapors coming out from a specially designed thermoelectrically heatable mini-furnace, assembled inside the cryostat (APD Cryogenics, model DE-202A) chamber, and a large excess of the matrix gas (argon, N60; xenon, N48, both obtained from Air Liquide) onto a CsI substrate cooled to 10 K (for argon matrices) and 20 K (for xenon matrices). The IR spectra were recorded with 0.5 cm^{-1} spectral resolution in a Mattson (Infinity 60AR Series) Fourier transform infrared spectrometer, equipped with a deuterated triglycine sulfate (DTGS) detector and a Ge/KBr beam splitter. Necessary modifications of the sample compartment of the spectrometer were done in order to accommodate the cryostat head and allow purging of the instrument by a stream of dry nitrogen, to remove water vapors and CO_2.

Irradiation of the matrices was carried out with unfiltered light from a 500 W Hg(Xe) lamp (Newport, Oriel Instruments), with output power set to 200 W, through the outer KBr windows of the cryostat (λ > 235 nm).

COMPUTATIONAL METHODS

The quantum chemical calculations were performed with Gaussian 03[51] at the DFT level of theory, using the split valence triple-ζ 6-311++G(d,p) basis set[52] and the three-parameter B3LYP density functional, which includes Becke's gradient exchange correction[53] and the Lee, Yang, and Parr correlation functional.[54]

Geometrical parameters of the different conformations were optimized using the geometry direct inversion of the invariant subspace (GDIIS) method.[55,56] Transition states were located using the synchronous transit-guided quasi-Newton (STQN) method.[57] In order to assist the analysis of the experimental spectra, vibrational frequencies and IR intensities were also calculated at the same level of approximation. The computed harmonic frequencies were scaled down by a single factor (0.9817) to correct them for the effects of basis set limitations, the neglected part of electron correlation, and anharmonicity effects. This factor was determined by simple linear fitting (with intercept fixed at zero) of the calculated wavenumbers to the experimental ones. The scaling procedure used was chosen mostly to achieve two goals: (1) to respect the potential energy distribution (i.e., mode composition) obtained directly from the MO calculations before scaling; this justifies the use of a single scale factor, and (2) to provide the best possible comparison with the experimental data; this justifies the choice for a fitting procedure instead of using a more standard scale factor extracted from general literature.

Normal coordinate analyses were undertaken in the internal coordinates space, as described by Schachtschneider and Mortimer,[58] using the optimized geometries and harmonic force constants resulting from the DFT(B3LYP)/6-311++G(d,p) calculations. The internal coordinates used in these analyses were defined according to the recommendations of Pulay et al.[59]

RESULTS AND DISCUSSION

Conformational Space of MCPIC. MCPIC is characterized by three conformationally relevant internal rotation axes defined around the $C_{14}-C_1$, C_3-C_6, and C_6-O_8 bonds (Figure 1). As in other carboxylic ester molecules,[60−65] internal rotation around the C_6-O_8 bond gives rise to *s-cis* and *s-trans* structures, with the *s-cis* species (C−C−O−C dihedral equal to 0°) being more stable than the *s-trans* forms by ca. 30 kJ mol^{-1}.[63−65] The latter species are then of no practical importance. On the other hand, internal rotations around the $C_{14}-C_1$ and C_3-C_6 bonds lead to different low energy conformers. A systematic investigation of the potential energy surface (PES) of the molecule was then undertaken by varying the $C_{15}-C_{14}-C_1-O_5$ and $C_2-C_3-C_6-O_8$

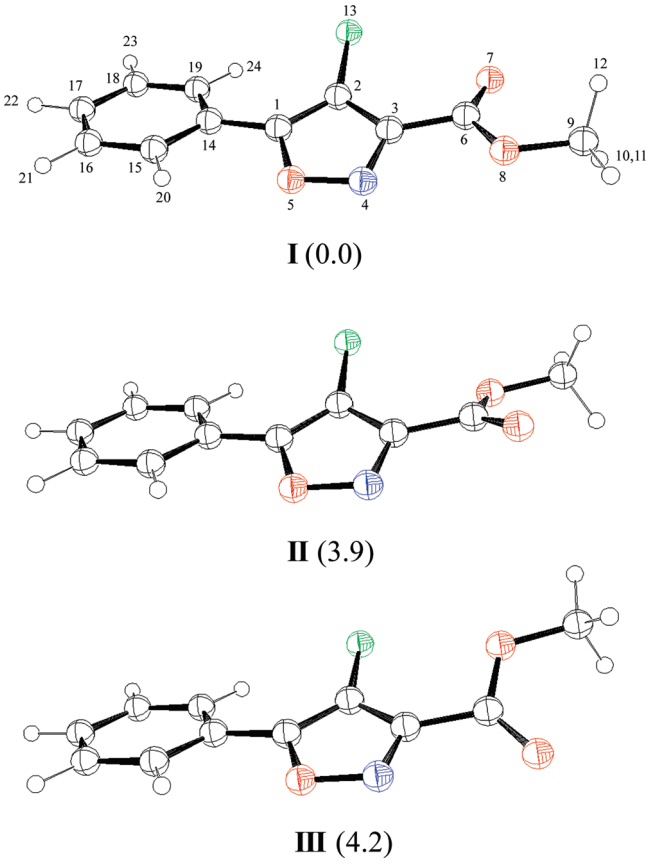

Figure 1. Low energy conformers of MCPIC, optimized at the DFT-(B3LYP)/6-311++G(d,p) level of theory, with atom numbering. Relative energies, including zero-point corrections ($\Delta E°$/ kJ mol^{-1}) are given in parentheses. The values of dipole moments (μ) for these conformers are 1.52, 4.09, and 4.09 D (1 D = 3.335 64 × 10^{-30} C m), respectively. Each conformer corresponds to four symmetry-related minima in the molecules' potential energy surface (see Figure 2). The complete calculated optimized geometries for the three conformers are given in Table S1 (Supporting Information). The picture was made using the Ortep-3 for Windows program (Farrugia, L. J. *J. Appl. Crystallogr.* **1997**, *30*, 565). Atoms color code: carbon, hydrogen, black; nitrogen, blue; chlorine, green; oxygen, red.

dihedral angles in steps of 30° and optimizing all remaining geometric parameters at each point.

Figure 2 presents the contour map of the DFT(B3LYP)/6-311++G(d,p) PES calculated as described above. Three sets of symmetry-equivalent energy minima were found on the PES, corresponding to three different conformers (**I**, **II**, and **III**; see Figure 1). According to calculations, conformers **II** and **III** are 3.9 and 4.2 kJ mol^{-1} higher in energy than the most stable form (calculated values including zero-point energy corrections; the corresponding relative energies from the bottom of the potential wells are 4.0 and 4.4 kJ mol^{-1}).

The calculated optimized geometries for the three conformers are given in Table S1 (Supporting Information). In all these conformers, the position of the phenyl group in relation to the isoxazole ring is nearly the same, the angle between the planes of the two rings being ca. 20° (more precisely, 18.5°, 19.0°, and 15.6° in **I**, **II**, and **III**, respectively; see Table S1). In the most stable conformer (**I**), the methyl ester group and the chlorine substituent of the isoxazole ring exhibit a nearly *trans* orientation, while in conformers **II** and **III** these groups exhibit a nearly *cis* arrangement: in conformer **I** the $C_2-C_3-C_6-O_8$ dihedral angle is ∼170°, while in conformers **II** and **III** this angle is ca. −25° and 25°, respectively. (Here we are considering the minima where the $C_{15}-C_{14}-C_1-O_5$ dihedral angle is ca. 20°, i.e., the minima corresponding to conformers **I** and **III** located in the first quadrant of the PES map shown in Figure 2, and that corresponding to conformer **II** located in the fourth quadrant. Other forms are related to these by symmetry.) The most stable conformer of MCPIC is similar to that determined by X-ray diffraction to be present in the crystal of the analogous bromo-substituted compound, 4-bromo-5-phenylisoxazole-3-carboxylate.[66] In that molecule, the angle between the phenyl and isoxazole ring was found to be 20.8° (compared to 18.5° now calculated for conformer **I** of MCPIC), and the $C_2-C_3-C_6-O_8$ dihedral angle 169.8° (compared to 169.3° for MCPIC).

In relation to the higher energy forms exhibiting an *s-trans* configuration about the C_6-O_8 bond, the calculations predicted the existence of only two conformers (forms **IV** and **V**; see Figure S1, Supporting Information). These conformers can be obtained from conformer **I** by rotation around the C_6-O_8 bond and, as already mentioned, are ca. 30 kJ mol^{-1} higher in energy than the most stable conformer. The conformationally relevant $C_{15}-C_{14}-C_1-O_5$, $C_2-C_3-C_6-O_8$, and $O_7{=}C_6-O_8-C_9$ dihedral angles in these high energy conformers were calculated as (14.9°, 137.0°, 173.1°) and (13.5°, −137.8°, −172.9°) for forms **IV** and **V**, respectively. No high energy conformers were found that could be obtained from rotation around the C_6-O_8 bond of forms **II** and **III**, i.e., exhibiting a $C_2-C_3-C_6-O_8$ dihedral angle in the ±25° region.

The main factors determining the relative stability of conformers **I**, **II**, and **III** can be guessed based on the fact that the conformers do not have the phenyl and isoxazole rings and the heavy atoms of the ester group in the same plane. This is a clear indication that repulsive interactions between both the phenyl and ester fragments and the chlorine substituent of the isoxazole ring are the key interactions determining the precise geometry of the conformers and their relative energies. The interaction between the phenyl group and the chlorine atom involves the closest phenyl hydrogen atom (H_{24}) and must be of steric nature, since electrostatic interactions would, in this case, favor the coplanarity of the two rings (phenyl and isoxazole). This interaction is of equal importance in conformers **I** and **II** and slightly more important in conformer **III**, as implied by the relative values for the dihedral angle between the planes of the two rings in the three conformers (18.5°, 19.0°, and 15.6°, for **I**, **II**, and **III**, respectively; see Figure 2 and Table S1), as well as H···Cl distances, which amount to 269.1 (**I**), 269.9 (**II**), and 265.9 (**III**) pm (sum of H and Cl van der Waals radii is ∼295 pm). The slightly higher energy of **III** compared with **II** is then partially accounted for by this interaction.

On the other hand, the interactions between the ester group and the chlorine atom are different in the three conformers and, besides determining the nonplanarity of the ester and isoxazole fragments (as measured by the $C_2-C_3-C_6-O_8$ dihedral angle; see Figure 2 and Table S1), must be responsible for their relative energies. In conformer **I**, it is the carbonyl oxygen (O_7) which interacts with the chlorine atom, whereas in conformers **II** and **III** the interaction involves O_8. These interactions are both steric and electrostatic. The calculated atomic polar tensor (APT) charges[67] for the three conformers are shown in Table 1. From this table, it can be noticed that O_8 is more negative than O_7, so

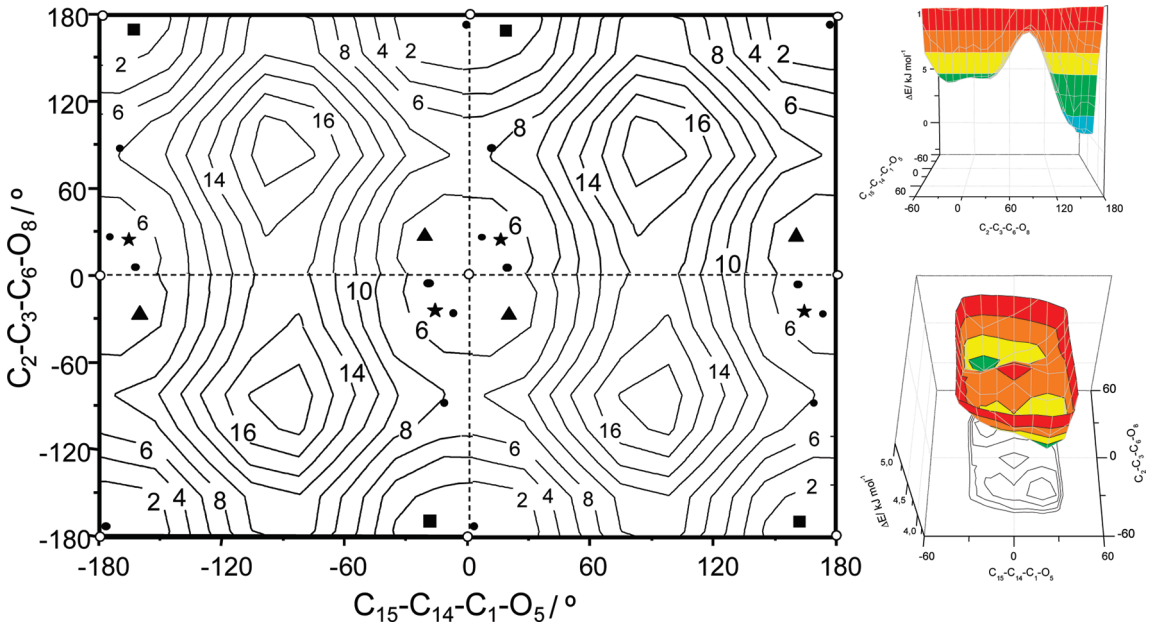

Figure 2. Left: B3LYP/6-311++G(d,p) potential energy map showing the position of the three low energy conformers of MCPIC. Each conformer correspond to four equivalent-by-symmetry minima; they are represented by squares (■, conformer **I**), triangles (▲, **II**), and stars (★, **III**). First-order transition states interconnecting the conformers are represented by black circles (●), and the C_s symmetry structures, corresponding to second-order transition states, by open circles (○). The isoenergy contour lines (kJ mol^{-1}) were obtained by fitting a grid of energy values with increments in the two scanned dihedral angles of 30°, interpolated according to the Renka−Cline method. All remaining geometric parameters were optimized at each point. See Figure 1 for conformers' structures and atom numbering. Right-top: PES profile along the $C_2-C_3-C_6-C_8$ coordinate, showing a possible pathway for interconversion between the three conformers. Right-bottom: expanded energy scale view of the PES in the vicinity of conformers **II** and **III**. In the two last panels, colors were used only for better visualization of the data.

that the Cl···O_8 electrostatic repulsion in **II** and **III** is more important than the Cl···O_7 electrostatic repulsion in **I**. This difference seems to be the main factor justifying the lower energy of **I** compared to **II** and **III**. In addition, the Cl···$O_{7/8}$ contact distances decrease in the order **I** (316.1 pm) > **II** (312.0 pm) > **III** (309.6 pm) (sum of O and Cl van der Waals radii is ∼327 pm), also contributing to make the Cl···O repulsive electrostatic interaction more important in the order **III** > **II** > **I**, and leading the Cl···O steric interaction to follow also the same trend.

On the whole, the H_{24}···Cl steric interactions and the Cl···$O_{7/8}$ electrostatic and steric interactions fully explain the relative energy of the three low energy conformers of MCPIC. It shall be noticed that in both conformers **I** and **II** the chlorine atom can move simultaneously apart from both H_{24} and $O_{7/8}$, since H_{24} and $O_{7/8}$ stay in the same side of the isoxazole ring (see Figure 1). On the other hand, in conformer **III**, the situation is different, since H_{24} and O_8 stay in opposite sides of the isoxazole ring, thus restricting in some amount the flexibility of the molecule to release energy by rotation about the $C_{14}-C_1$ and C_3-C_6 bonds. This is consistent with the smaller dihedral angles between the two rings and about the C_3-C_6 bond in conformer **III**.

The pathways for interconversion between the three low energy conformers of MCPIC were also evaluated in this study. Two preliminary observations must be stressed. (i) The first one is that it is clear from Figure 2 that, for each conformer, two symmetry-equivalent minima exist in two different valleys on the PES. These two valleys are defined by values of the $C_{15}-C_{14}-C_1-O_5$ dihedral angle in the ranges (−30°, 30°) and (150°, −150°) and extend the full range of the $C_2-C_3-C_6-O_8$ dihedral angle, being symmetrically equivalent. The two valleys are separated by barriers larger than 10 kJ mol^{-1}. (ii) The second preliminary observation is that the possible C_s symmetry structures, where the two rings and the heavy atoms of the ester fragment of MCPIC are in the same plane, correspond to second-order transition states.

Within the same valley [let us consider that depicted in the central part of Figure 2, corresponding to $C_{15}-C_{14}-C_1-O_5$ in the (−60°, 60°) range and shown in an extended energy scale in a separate graph in Figure 2], we found that the two equivalent-by-symmetry structures corresponding to conformer **I** can be interconverted directly to each other by crossing a barrier of 0.3 kJ mol^{-1} (0.2 kJ mol^{-1} if zero-point corrections are taken into account), following two symmetry equivalent pathways whose transition states have the $C_{15}-C_{14}-C_1-O_5$ and $C_2-C_3-C_6-O_8$ dihedral angles equal to −0.8° and 172.8° or 0.8° and −172.8°. These two first-order transition states are symmetrically located in relation to the planar second-order transition state with $C_{15}-C_{14}-C_1-O_5$ and $C_2-C_3-C_6-O_8$ dihedral angles equal to 0° and 180° (see Figure 2).

On the other hand, the symmetry-equivalent forms of both conformers **II** and **III** cannot be converted directly to each other, since no first-order transition states exist between those forms. Direct conversion would imply simultaneous rotation about the $C_{14}-C_1$ and C_3-C_6 bonds, passing the second- order transition state defined by $C_{15}-C_{14}-C_1-O_5$ and $C_2-C_3-C_6-O_8$ dihedral angles equal to 0° (see Figure 2). Conformers **II** and **III** can, alternatively, be easily converted into each other by rotation around either the $C_{14}-C_1$ or C_3-C_6 bonds. Though the barriers associated with these two pathways are both very small, the one implying a rotation around the C_3-C_6 bond is predicted to be slightly lower than that associated with the rotation around the $C_{14}-C_1$ bond: zero-point corrected values, $\Delta E_o^{\#}{}_{(\mathbf{III}\rightarrow\mathbf{II})}$ = 0.1 vs

dx.doi.org/10.1021/jp110705c |*J. Phys. Chem. A* 2011, 115, 1199–1209

Table 1. DFT(B3LYP)/6-311++G(d,p) Calculated Atomic Polar Tensor (APT) Charges on Atoms for Conformers I, II, and III of MCPIC[a]

	APT charges/e		
atom	I	II	III
C_1	0.402	0.412	0.408
C_2	0.049	0.046	0.048
C_3	0.070	0.075	0.070
N_4	−0.150	−0.157	−0.157
O_5	−0.433	−0.421	−0.420
C_6	1.354	1.336	1.342
O_7	−0.739	−0.763	−0.766
O_8	−0.932	−0.890	−0.891
C_9	0.518	0.505	0.505
H_{10}	−0.019	−0.015	−0.017
H_{11}	−0.018	−0.017	−0.015
H_{12}	0.009	0.012	0.012
Cl_{13}	−0.157	−0.167	−0.167
C_{14}	0.015	0.010	0.017
C_{15}	−0.061	−0.060	−0.064
C_{16}	−0.040	−0.041	−0.041
C_{17}	−0.035	−0.035	−0.036
C_{18}	−0.041	−0.039	−0.038
C_{19}	−0.045	−0.044	−0.047
H_{20}	0.074	0.071	0.074
H_{21}	0.035	0.034	0.034
H_{22}	0.039	0.039	0.039
H_{23}	0.034	0.034	0.034
H_{24}	0.075	0.075	0.077

[a] See Figure 1 for atom numbering. $1e = 1.602\,176\,46 \times 10^{-19}$ C.

0.2 kJ mol^{-1} (0.4 vs 0.6 kJ mol^{-1} in the opposite direction); values without zero-point corrections, $\Delta E^{\#}_{(\mathbf{III}\rightarrow\mathbf{II})}$ = 0.1 vs 0.3 kJ mol^{-1} (0.4 vs 0.6 kJ mol^{-1} in the opposite direction).

Finally, both conformers **II** and **III** can also be converted into the most stable form. Interestingly, the two conversion pathways were found to include a common first-order transition state (see Figure 2), which leads to **II** → **I** and **III** → **I** energy barriers of 3.9 and 3.6 kJ mol^{-1}, respectively (7.8 kJ mol^{-1} in the reverse direction) (zero-point corrected values; noncorrected values are 4.3 kJ mol^{-1} (**II** → **I**), 4.0 kJ mol^{-1} (**III** → **I**), and 8.3 kJ mol^{-1} (**I** → **II**/**III**).

Matrix Isolation IR Spectra of MCPIC (As-Deposited Matrices). All conformers of MCPIC belong to the C_1 symmetry point group, possessing 66 fundamental vibrations, all of them active in the infrared. In order to interpret the experimental spectra of the compound, the B3LYP/6-311++G(d,p) IR spectra of its experimentally relevant low energy conformers were obtained and normal coordinate analysis calculations were performed. The definition of the internal coordinates used in the vibrational analysis is provided in Table S2 (Supporting Information). The complete list of calculated wavenumbers, IR intensities, and potential energy distributions resulting from the normal-mode analyses are presented in Tables S3 and S4 (Supporting Information).

As discussed in detail in the previous section, the three low energy conformers of MCPIC have relative energies of 0.0 (**I**), 3.9 (**II**), and 4.2 (**III**) kJ mol^{-1}. At the sublimation temperature used to deposit the matrices (50 °C), the estimated Boltzmann populations of these conformers are 69.2%, 16.4%, and 14.4%, respectively. However, the energy barriers associated with the **III** → **II** conformational isomerization are very low (<0.3 kJ mol^{-1}). Energy barriers of this magnitude are known[68−72] to be easily overcome during deposition of matrices under the experimental conditions used in this study. The gas being deposited is hot, and the energy dissipated and made available during the landing of the molecules onto the cold substrate is enough to allow the barrier to be surpassed. In the present case, this can be expected to lead to relaxation of the higher energy conformer **III** into the lower energy conformer **II**. Hence, we can expect exclusive observation of conformers **I** and **II** in the as-deposited matrices of MCPIC. If no conversion from **II** to **I** takes place during

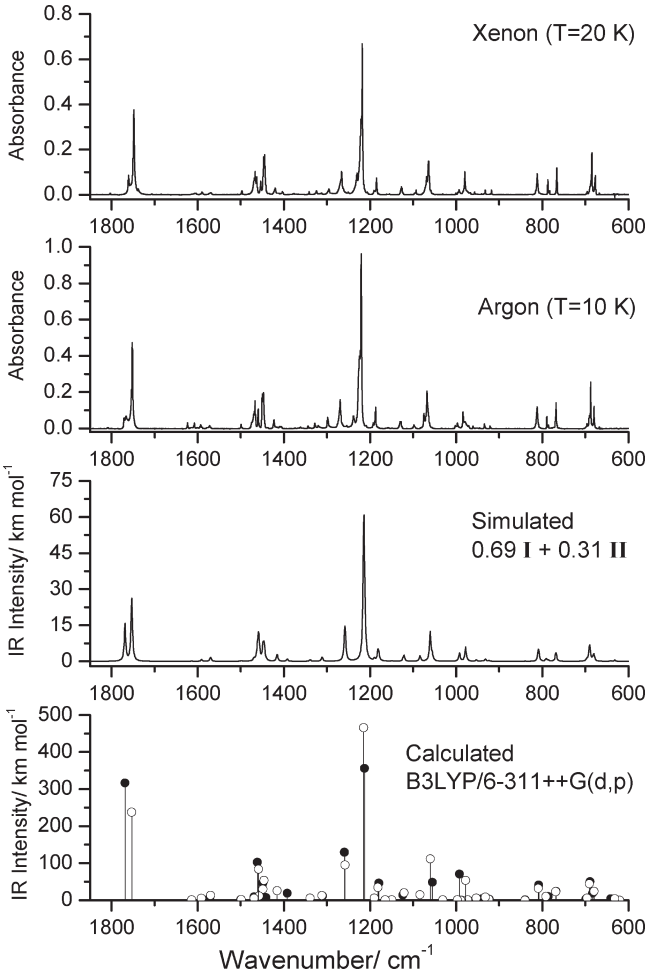

Figure 3. Top (two panels): infrared spectra of MCPIC isolated in solid argon and xenon (as-deposited matrices; temperature of the deposited vapor: 50 °C; substrate temperature during deposition: argon, 10 K; xenon, 20 K). Bottom: DFT(B3LYP)/6-311++G(d,p) calculated infrared spectra of MCPIC conformers **I** (open circles, ○) and **II** (black circles, ●) shown as stick spectra (wavenumbers scaled by 0.9817). Middle: simulated spectra of the expected conformational mixture at 50 °C, built by adding the calculated spectra of conformers **I** and **II** with intensities scaled by their predicted populations (69% for conformer **I** and 31% for conformer **II**; see text). In the simulated spectra, bands were represented by Lorentzian functions centered at the calculated wavenumbers (scaled by 0.9817) and with fwhm (full width at half-maximum) equal to 4 cm^{-1}.

deposition, the population of conformer **II** in the matrices should correspond to the sum of those of conformers **II** and **III** in the vapor being deposited, i.e., 30.8%.

Figure 3 shows the infrared spectra of MCPIC isolated in both argon and xenon matrices (sublimation temperature, 50 °C; substrate temperature during deposition: argon, 10 K; xenon, 20 K). The B3LYP/6-311++G(d,p) theoretically predicted spectra of conformers **I** and **II** are also presented in this figure (in the format of stick spectra), as well as the simulated spectra of the expected conformational mixture at 50 °C, built up by adding the calculated spectrum of conformers **I** and **II** with intensities scaled by their predicted populations (69% for conformer **I** and 31% for conformer **II**; see text).

The experimental spectra are well reproduced by the simulated spectrum, though it is clear that the population of conformer **II** is smaller than expected taking into account its predicted population in the vapor of the compound at 50 °C. It can also be noticed that the population of **II** is smaller in the xenon than in the argon matrix. Indeed, the relative populations of the conformers present in the matrices were estimated from the observed integral bands intensities in the carbonyl stretching region (normalized by the calculated intensities of the conformers). According to this estimation, conformer **I** accounts for 86.1% of the total population in argon matrix and conformer **II** for the remaining 13.9%, whereas in the xenon matrix these values change to 90.4% (**I**) and 9.6% (**II**). All these results are consistent with the occurrence of two isomerization processes during deposition of the matrices: (i) conformer **III** is fully converted to form **II**, as expected taking into account the very low energy barriers for the **III** → **II** isomerization (<0.3 kJ mol^{-1}), and it is not present either in the argon or in the xenon matrix; (ii) conformer **II** is partially converted to the most stable conformer **I**. As discussed above, the last process has a predicted gas phase barrier of ca. 4 kJ mol^{-1}, which is still low enough to be accessible during deposition of the matrices, in particular in the case of the xenon matrix, where the temperature of the substrate during deposition was higher. A higher temperature of the substrate during deposition facilitates the conformational cooling.[68−72] Moreover, xenon has also been shown to facilitate conformational cooling in relation to argon.[69,70]

Annealing of the matrices to higher temperatures was also undertaken, in order to check the possibility of conformer **II** to be converted into conformer **I** after the matrix is formed. However, no significant changes could be observed in the spectra that could be unequivocally ascribed to the **II** → **I** conversion in the accessible range of temperatures (at ca. 30 K, the argon matrix started to deteriorate and aggregation of the compound started to be important; the same happened in the case of the xenon matrix at ca. 60 K). If we take into account the Barnes relationship between the temperature and the conversion barriers,[68] the nonobservation of the **II** → **I** conversion until ca. 60 K indicates that the isomerization barrier for this process in the matrices must considerably increase to ca. 14−17 kJ mol^{-1}. Since this isomerization implies rotation of a voluminous fragment (the $COOCH_3$ moiety), such increase in the barrier to internal rotation in going from the gas phase to the solid state matrix could indeed be anticipated. In a matrix, this process would require extensive rearrangement of the matrix host, which is an energetically demanding process contributing to the increase of the effective barrier and, in the present case, precluding observation of the isomerization reaction.

The assignment of the bands in the experimental spectra was strongly aided by the excellent agreement between the experimental and the calculated data. The observed bands are mostly due to the most abundant conformer **I**, though in most of the cases they shall also contain a minor contribution from the less abundant conformer **II**, since the spectra of the two forms are quite similar (see Figure 3, bottom panel). The proposed assignments are presented in Table 2. A few bands (or prominent shoulders) could be tentatively ascribed to conformer **II**, besides those originated in the carbonyl stretching mode of this conformer, appearing at 1771/1767 cm^{-1} in argon and 1760 cm^{-1} in xenon, whose assignment is unequivocal. Such bands appear at 1472/1470 (δC−H1, νIsox1), 1410/1407 (νIsox4), 1272 (shoulder; νIsox2), 1239/1227/1224 (νC−O), 1129 (νIsox5, νIsox1), 1066/1063 (δIsox2), and 1002/1000/997/992 (νIsox5) cm^{-1} in argon and, correspondingly, at 1470/1469, 1404/1401, 1269 (shoulder), 1234/1232/1230/1221, 1124, 1064/1058, and 1002/1000/996/993 cm^{-1} in xenon (see Table S2 in the Supporting Information for designation of the vibrational modes and also Table S4).

Photolysis Experiments (In Situ UV Irradiation with λ > 235 nm). In situ UV irradiation experiments were carried out to study the photochemistry of MCPIC in argon and xenon matrices. Upon broad-band UV irradiation (λ > 235 nm) of the matrix isolated compound, significant changes occurred in the infrared spectrum, with bands due to MCPIC decreasing in intensity while new bands due to photoproducts emerged (Figures 4 and 5). The obtained results were identical in both argon and xenon matrices, with the difference that the observed reactions were found to be considerably faster in the latter matrix, indicating that triplet states are involved in the photoprocesses,[71,73] as it has also been suggested before based on the relative quantum yields for isoxazole → oxazole conversion of the studied compound and its bromo-substituted analogue in solution,[74] and acetone-sentitized conversion of 3-acetyl-5-methylisoxazole into the corresponding oxazole in different solvents.[75] The involvement of triplet states in the photoisomerization of isoxazole to oxazole has also been predicted theoretically.[45,76] In a xenon matrix, after 90 min of irradiation ca. 90% of the initially deposited MCPIC was transformed into other species, while in argon matrix only ca. 50% of the reactant was consumed. Below, we will concentrate the discussion on the results obtained in the xenon matrix.

Figure 4 (middle panel) shows the difference infrared spectrum obtained by subtracting the spectrum of the MCPIC xenon matrix irradiated during 90 min (λ> 235 nm) and the spectrum of the as-deposited MCPIC xenon matrix. The negative bands shown in this spectrum correspond to the bands of the reactant whose IR spectrum in a freshly deposited xenon matrix is also shown in the figure as a reference (bottom panel). The spectrum shown in the top panel of Figure 4 is the infrared spectrum of methyl 4-chloro-5-phenyl-1,3-oxazole-2-carboxylate (MCPOC) deposited in xenon matrix at 20 K in a different experiment. It is clear from the data shown in that figure that the main product from the photolysis (λ > 235 nm) of matrix-isolated MCPIC is its isomeric oxazole, MCPOC.

It is also clear from Figure 4 that, in addition to the bands due to MCPOC, other bands appear in the spectrum of the photolyzed matrix (positive bands in the difference spectrum shown in Figure 4, e.g., in the 1800−1650 cm^{-1} region, and at 1601, 1584, 1256, 1240, and ca. 705 cm^{-1}), which must be assigned to different photoproducts. In order to allow for a clear examination of these bands, the spectrum of MCPOC was subtracted (multiplied by an appropriated intensity factor) from the difference spectrum presented in

Table 2. Experimental (Matrix-Isolation) and Calculated Vibrational Data for MCPIC with Vibrational Assignments Based on the Results of Normal Coordinate Analysis[a]

experimental		calculated		
Ar matrix	Xe matrix	conformer **I**		
ν	ν	ν	I	approximate description
3120	3114	3159	1.7	ν(C−H1)
3105	3096	3146	3.0	ν(C−H5)
3090/3081	3084	3132	16.9	ν(C−H2)
3070	3065/3060	3121	9.9	ν(C−H3)
3046/3035/3030	3040	3107	11.0	νCH_3 as′
3014	3027	3070	16.3	νCH_3 as″
2964	2994	2998	34.3	νCH_3 s
1755/1752	1754/1748/1738	1753	237.5	νC═O
1601	n.obs.	1614	1.0	νPh3
1593	1590/1586	1591	4.8	νPh4
1573	1570	1570	13.1	νIsox3
1499	1497	1499	1.8	δ(C−H4)
n.obs.	1482	1469	5.2	δCH_3 as′
1467	1466/1463	1459	83.7	δ(C−H1), νIsox1
1459	1453	1457	11.6	δCH_3 as″
1450	1445	1448	29.7	δCH_3 s
1448/1447	1445/1443(sh)	1446	53.1	νIsox2
1423	1423(sh)/1420	1416	25.5	νIsox4
1344/1340	1344(sh)/1341	1339	5.6	δ(C−H2)
1328/1320/1318/1315	1324/1315/1313	1312	12.1	νPh2
1269/1299[b]	1297/1275/1266/1262[b]	1258	94.7	$\nu(C-C_{IR})$
1221	1218	1215	465.5	νC−O
1192	1191/1189	1190	5.8	δ(C−H3)
1189(sh)/1187/1182	1185/1183/1180	1182	34.2	$\gamma CH_3'$
1164	1161	1165	0.5	δ(C−H5)
1159	1155	1149	0.9	$\gamma CH_3''$
1130	1127	1121	19.6	νIsox1
1098/1096(sh)	1096(sh)/1093	1084	14.7	νPh6
1082/1079/1075/1073(sh)	1071/1069	1060	111.5	δIsox2
1034	1031	1031	0.5	νPh5
984/980/971	985(sh)/980/973/967	978	53.5	νIsox5
n.obs.	n.obs.	973	1.0	γ(C−H4)
961/957	957	953	5.5	$\nu(O-CH_3)$
934	933/931	932	8.1	$\nu(O-CH_3)$
921/920(sh)/919(sh)	920/918	924	2.6	γ(C−H5), γ(C−H1)
841	839	840	0.4	γ(C−H1)
814(sh)/812	812	809	31.9	δ(OCO)
790/788(sh)/786	787/784	791	9.5	γ(C═O)
769(sh)/768	766	769	23.2	γ(C−H3)
696/692(sh)/691	695/691/689/687	696	6.1	δPh3
688/684	685/681	691	44.0	τPh1
680	677	680	23.4	τIsox1
579	575	573	1.1	w(Isox-E), w(Isox-Ph), w(C−Cl)
486/485/477	484/482	485	2.7	γ(Ph-Isox)

[a] Wavenumbers (cm^{-1}, scaled by 0.9817); calculated intensities (km mol^{-1}); ν, bond stretching; δ, bending; γ, rocking; w, wagging; τ, torsion; s, symmetric; as, antisymmetric; IR, inter-ring; Isox, isoxazole ring; Ph, phenyl ring; E, ester; sh, shoulder; n.obs., not observed; see Table S2 (Supporting Information) for definition of internal coordinates and Table S3 for potential energy distributions. [b] Fermi resonance with τPh1 + (w(Isox-E), w(Isox-Ph), w(C−Cl)).

dx.doi.org/10.1021/jp110705c |J. Phys. Chem. A 2011, 115, 1199–1209

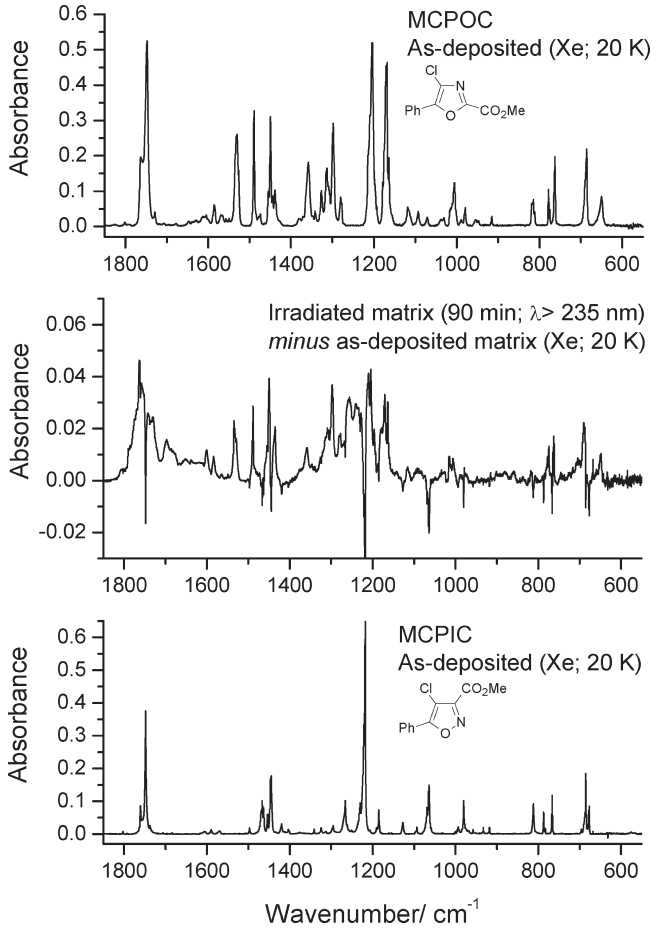

Figure 4. Bottom: IR spectrum (1850−550 cm^{-1} range) of MCPIC in a xenon matrix (as deposited; 20 K). Middle: IR difference spectrum (λ > 235 nm irradiated xenon matrix during 90 min minus as-deposited matrix). Top: IR spectrum of MCPOC in a xenon matrix (as-deposited; 20 K).

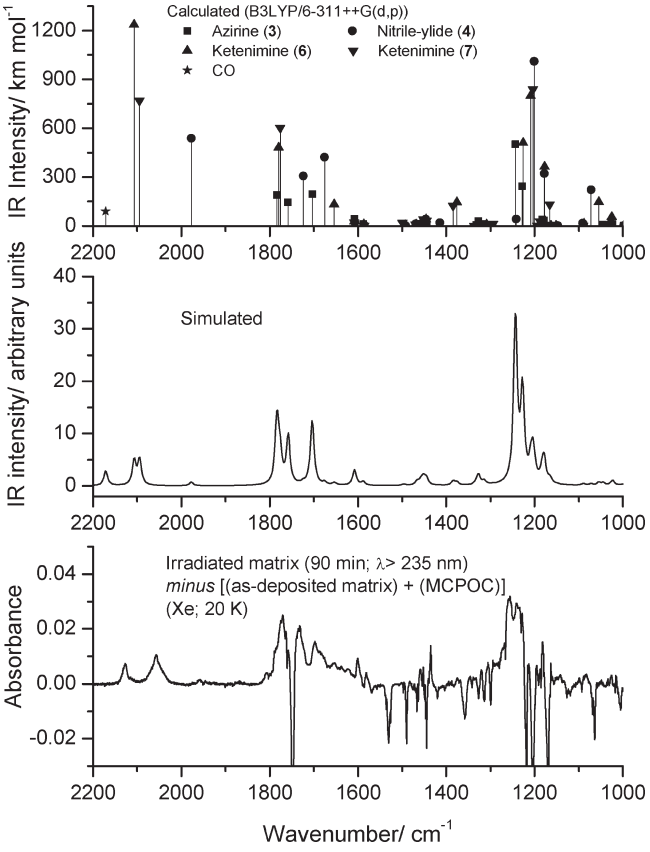

Figure 5. Top: B3LYP/6-311++G(d,p) calculated IR stick spectra for other than MCPOC observed photoproducts of MCPIC (wavenumbers scaled by 0.9817). Middle: simulated IR spectrum built from the B3LYP/6-311++G(d,p) calculated spectra shown in the top panel (intensities of the different species were arbitrarily scaled in order to obtain the best match with the experimental data; bands were simulated by Lorentzian functions centered at the calculated frequencies and with fwhm equal to 10 cm^{-1}). Bottom: IR difference spectrum (2300−1000 cm^{-1} range) obtained by subtracting the difference spectrum shown in Figure 4 (λ > 235 nm irradiated xenon matrix during 90 min minus as-deposited matrix) and the spectrum of MCPOC in a xenon matrix (as-deposited; 20 K) multiplied by an appropriated intensity factor. The bands pointing down in this spectrum correspond to both MCPIC and MCPOC.

Figure 4. The obtained new difference spectrum is shown in Figure 5. In this figure, the presented spectral region corresponds to that where the strongest and most characteristic bands of other than the oxazole photoproduct are observed.

The identification of the photoproducts contributing to the positive bands shown in Figure 5 was done both by calculating the IR spectra of a series of possible photoproducts at the DFT(B3LYP)/6-311++G(d,p) level of theory and, whenever available, by comparing the position of the bands with characteristic bands of similar molecules.

According to the previously proposed mechanism for the photochemical isoxazole−oxazole rearrangement[46−48], the primary photoproduct, resulting from cleavage of the weakest bond in isoxazole, the N−O bond, should be the vinyl nitrene (**2**, in Scheme 1, where for the present molecule R_1 is a phenyl group, R_2 a chlorine substituent, and R_3 the methyl ester fragment). Such a species has never been experimentally detected, and it is supposed to rearrange very easily to the closed ring 2*H*-azirine (**3**, in Scheme 1). Hence, the first molecule here considered as a possible contributing species to the spectrum of the photolyzed matrix (besides MCPOC) was the azirine methyl 2-benzoyl-2-chloro-2*H*-azirine-3-carboxylate (MBCAC). Substituted 2*H*-azirines with a methyl ester group have characteristic intense bands around 1780, 1750, and 1250 cm^{-1}, corresponding to the symmetric and antisymmetric combination of the νC═N and νC═O coordinates, and the νC−O stretching mode, respectively.[41,73,77] The spectrum calculated in this study for the most stable conformer of MBCAC is presented (in the form of a stick spectrum) in Figure 5 and accounts for most of the positive bands of the difference spectrum shown in this figure, allowing for unequivocal identification of MBCAC in the spectrum of the photolyzed matrix.

The identification of the remaining photoproducts was mainly made on the basis of the bands appearing in the 2300−1900 cm^{-1} spectral region, which is a clean region in the spectra of MCPIC, MCPOC, and MBCAC.

The first band in this region is observed at 1955 cm^{-1} and appears at the characteristic wavenumber of the antisymmetric stretching of the CNC fragment of a nitrile-ylide.[77,78] The intensity of this band is low, and all other bands predicted by

Scheme 2

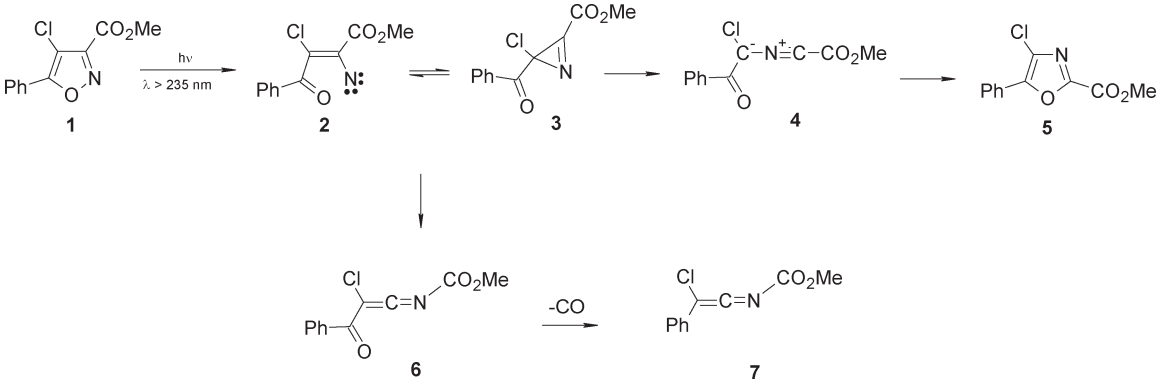

the calculations to be intense for the nitrile-ylide resulting from MCPIC (**4** in Scheme 1) are expected to appear in regions where either MCPOC or MBCAC also absorb. Hence, this corresponds to the sole band unequivocally ascribable to the nitrile-ylide. However, its very characteristic wavenumber[77,78] ensures certainty in the identification of this species. Together with the observation of the azirine MBCAC, the observation of the nitrile-ylide in the spectrum of the matrix resulting from the photolysis of MCPIC (see also Figure 5) confirms the previously proposed mechanism for the photochemical isoxazole → oxazole rearrangement.[46−48]

The other bands found in the 2300−1900 cm^{-1} spectral region of the spectrum of the photolyzed matrix result from species photoproduced from the vinyl nitrene and/or the azirine in alternative competing photochemical pathways (see Scheme 2).

The band observed at 2057 cm^{-1} is characteristic of the ketenimine νC═C═N antisymmetric stretching mode[77−79] and can then be ascribed to the ketenimine **6** (Scheme 2), which can result from rearrangements of both the azirine and vinyl nitrene intermediates. In Figure 5 it can be seen that the calculated wavenumber for the ketenimine **6** νC═C═N antisymmetric stretching mode fits nicely that of the experimentally observed band here ascribed to this mode. Contrarily to nitrile-ylides, which result from the usually preferred photochemical breakage of the C−C bond of the azirine ring, ketenimines result from cleavage of the C−N bond. Nevertheless, the photochemical formation of ketenimines from 2*H*-azirines (in particular those substituted by a methyl ester group in the position 3 of the ring) has been observed.[71,73−80] The subsequent decarbonylation of the ketenimine **6** can account for the observation of the characteristic band of CO in the photolyzed MCPIC matrices. This band is observed at in the 2139−2119 cm^{-1} range, with maximum at 2127 cm^{-1}. Monomeric CO isolated in a xenon matrix gives rise to a band at 2133 cm^{-1}.[81,82] The product formed together with CO, which is also a ketenimine (**7**, in Scheme 2), shall also contribute to the band at 2057 cm^{-1} (see Figure 5). Decarbonylation of conjugated ketenimines like **6** has also been previously described.[71,73]

■ CONCLUSIONS

Methyl 4-chloro-5-phenylisoxazole-3-carboxylate was isolated in cryogenic matrices of noble gases (argon, xenon), and the preferred conformations assumed by the monomer of the compound were probed by infrared spectroscopy, supported by theoretical calculations undertaken at the DFT(B3LYP)/6-311++G(d,p) level of approximation. The theoretical potential energy surface revealed the existence of three low energy conformers, the most stable form, **I**, being characterized by $C_{15}-C_{14}-C_1-O_5$, $C_2-C_3-C_6-O_8$, and $O_7=C_6-O_8-C_9$ dihedral angles of 169.8°, 18.5°, and −1.2°, being similar to the conformer present in the crystal of the analogous bromo-substituted compound, 4-bromo-5-phenylisoxazole-3-carboxylate.[66] Conformers **II** and **III** differ from **I** fundamentally in the orientation of the ester fragment and are 3.9 and 4.2 kJ mol^{-1} higher in energy than the most stable conformer. The $H_{24}\cdots Cl$ steric interactions and $Cl\cdots O_{7/8}$ electrostatic and steric interactions were found to explain the relative energy of the three conformers.

Conformers **I** and **II** were observed in the matrix isolation experiments, whereas conformer **III** was found to be totally converted into conformer **II** during deposition of the matrices. These results are in consonance with the very low energy barrier associated with the **III** → **II** conversion (<0.3 kJ mol^{-1}), which can be easily overcome during deposition of the matrices. Moreover, partial conversion of **II** into **I** during matrix deposition was also observed, a result that is also consistent with the moderately low predicted isomerization barrier for the **II** → **I** conversion (ca. 4 kJ mol^{-1}). On the other hand, annealing of the matrices up to 60 K (in xenon) did not promote any conversion of **II** into **I**, which points to a much larger barrier for this process in the solid matrix environment.

The assignment of the bands observed in the IR spectra (3500−400 cm^{-1} range) of MCPIC in both argon and xenon matrices was undertaken, aided by the excellent agreement between the experimental and the calculated spectroscopic data.

Broad-band UV (λ > 235 nm) irradiation of matrix-isolated MCPIC was found to lead to the corresponding oxazole, methyl 4-chloro-5-phenyl-1,3-oxazole-2-carboxylate, as final photoproduct. In agreement with the mechanism for the isoxazole → oxazole photoisomerization previously proposed,[40−45] the expected azirine and nitrile-ylide intermediates could be identified spectroscopically in the present study in the photolyzed matrices.

■ ASSOCIATED CONTENT

Supporting Information. Figure S1, high energy conformers of MCPIC optimized at the B3LYP/6-311++G(d,p) level of theory; Table S1, the calculated geometries for MCPIC

low energy conformers **I**, **II**, and **III**; Table S2, definition of internal coordinates used in the normal-mode analysis of MCPIC; Tables S3 and S4, B3LYP/6-311++G(d,p) calculated spectroscopic data and results of normal coordinate analysis for the two most stable, experimentally relevant conformers of MCPIC (forms **I** and **II**). This material is available free of charge via the Internet at http://pubs.acs.org.

AUTHOR INFORMATION

Corresponding Author
*E-mail rfausto@ci.uc.pt.

ACKNOWLEDGMENT

These studies were partially funded by the Portuguese Science Foundation (Project No. FCOMP-01-0124-FEDER-007458, cofunded by QREN-COMPETE-UE, and Grants No. SFRH/BD/29698/2006 and SFRH/BD/28844/2006). The authors also thank Milipeia Computer Centre (research project "Computação Avançada em Espectroscopia Molecular"), MinCyt-FCT (bilateral grant PO/09/18), and the Iberoamerican Program for the Development of Science and Technology, CYTED (Network 198RT0362). A.G.-Z. is a member of the Research Career CONICET, Argentina.

REFERENCES

(1) Sechi, M.; Sannia, L.; Carta, F.; Palomba, M.; Dallocchio, R.; Dess, A.; Derudas, M.; Zawahir, Z.; Neamati, N. *Antivir. Chem. Chemother.* **2005**, *16*, 41–61.
(2) Diana, G. D.; Cutcliffe, D.; Oglesby, R. C.; Otto, M. J.; Mallamo, J. P.; Akullian, V.; McKinlay, M. A. *J. Med. Chem.* **1989**, *32*, 450–455.
(3) Youn, H. S.; Lee, E. J.; Lee, J. E.; Park, W.-K.; Baek, Du-J.; Cho, Y. S.; Koh, H. Y.; Choo, H.; Pae, A. N. *Bull. Korean Chem. Soc.* **2009**, *30*, 1873–1876.
(4) Calí, P.; Nærum, L.; Mukhija, S.; Hjelmencrantz, A. *Bioorg. Med. Chem. Lett.* **2004**, *14*, 5997–6000.
(5) Tatee, T.; Kurashige, S.; Shiozawa, A.; Narita, K.; Takei, M.; Ito, S.; Miyazaki, H.; Yamanaka, H.; Mizugaki, M.; Sakamoto, T.; Fukuda, H. *Chem. Pharm. Bull.* **1986**, *34*, 1634–1642.
(6) Habeeb, A. G.; Rao, P. N. P.; Knaus, E. E. *Drug Develop. Res.* **2000**, *51*, 273–286.
(7) Rapposelli, S.; Lapucci, A.; Minutolo, F.; Orlandini, E.; Ortore, G.; Pinza, M.; Balsamo, A. *Il Farmaco* **2004**, *59*, 25–31.
(8) Saunders, J. C.; Williamson, W. R. N. *J. Med. Chem.* **1979**, *22*, 1554–1558.
(9) Eddington, N. D.; Cox, D. S.; Roberts, R. R.; Butcher, R. J.; Edafiogho, I. O.; Stables, J. P.; Cooke, N.; Goodwin, A. M.; Smith, C. A.; Scott, K. R. *Eur. J. Med. Chem.* **2002**, *37*, 635–648.
(10) Al-Omran, F.; El-Khair, A. A. *J. Heterocycl. Chem.* **2004**, *41*, 327–333.
(11) Simoni, D.; Roberti, M.; Invidiata, F. P.; Rondanin, R.; Baruchello, R.; Malagutti, C.; Mazzali, A.; Rossi, M.; Grimaudo, S.; Capone, F.; Dusonchet, L.; Meli, M.; Raimondi, M. V.; Landino, M.; D'Alessandro, N.; Tolomeo, M.; Arindam, D.; Lu, S.; Benbrook, D. M. *J. Med. Chem.* **2001**, *44*, 2308–2318.
(12) Shin, K. D.; Lee, Mi-Y.; Shin, D.-S.; Lee, S.; Son, K.-H.; Koh, S.; Paik, Y.-Ki; Kwon, B.-M.; Han, D. C. *J. Biol. Chem.* **2005**, *280*, 41439–41448.
(13) Carr, J. B.; Durham, H. G.; Hass, D. K. *J. Med. Chem.* **1977**, *20*, 934–939.
(14) Haugwitz, R. D.; Angel, R. G.; Jacobs, G. A.; Maurer, B. V.; Narayanan, V. L.; Cruthers, L. R.; Szanto, J. *J. Med. Chem.* **1982**, *25*, 969–974.
(15) Goulding, K. H.; Yung, K.-M.; Hall, A. M.; Cremlyn, R. J. W. *Pesticide Sci.* **1983**, *14*, 158–166.
(16) Pallett, K. E.; Cramp, S. M.; Little, J. P.; Veerasekaran, P.; Crudace, A. J.; Slater, A. E. *Pesticide Manag. Sci.* **2001**, *57*, 133–142.
(17) Baker, A. D.; Betteridge, D.; Kemp, N. R.; Kirby, R. E. *Anal. Chem.* **1970**, *42*, 1064–1073.
(18) Liu, Y.; Cui, Z.; Liu, B.; Cai, B.; Li, Y.; Wang, Q. *J. Agric. Food Chem.* **2010**, *58*, 2685–2689.
(19) Naka, K.; Horii, E.; Chujo, Y. *Polym. J.* **2000**, *32*, 73–74.
(20) Shang, Y.-J.; Wang, Y.-G. *Tetrahedron Lett.* **2002**, *43*, 2247–2249.
(21) Abdel-Hafiz, S. A.; El-Kholy, Y. M. *Pigm. Resin Technol.* **1995**, *24*, 13–16.
(22) Al-Abdallah, M. M.; Abu-Orabi, S. T. *Anti-Corros. Methods Mater.* **1989**, *36*, 4–6.
(23) Lang, S. A., Jr.; Lin, Y.-I. In Katristzky, A. R., Rees, C. W., Series Eds.; Potts, K. T., Ed.; *Comprehensive Heterocyclic Chemistry*, Pergamon: Oxford, U.K., 1984; Vol. 6, Part 4B, Chapter 4.16, pp 1−130.
(24) Silva, L.; Gallardo, H.; Magnago, R. F.; Begnini, I. M. *Mol. Cryst. Liq. Cryst.* **2005**, *432*, 1–13.
(25) Santos, D. R.; Oliveira, A. G. S.; Coelho, R. L.; Begnini, I. M.; Magnago, R. F.; Silva, L. *Arkivoc* **2008**, *17*, 157–166.
(26) Uno, T.; Machida, K.; Hanai, K. *Chem. Pharm. Bull.* **1966**, *14*, 756–762.
(27) Takasuka, M.; Nakai, H. *Vib. Spectrosc.* **2001**, *25*, 197–204.
(28) McGlone, S.; Bauder, A. *J. Chem. Phys.* **1998**, *103*, 5383–5392.
(29) Stiefvater, O. L. *J. Chem. Phys.* **1975**, *63*, 2560–5569.
(30) Jezierska, A.; Panek, J.; Ryng, S. *J. Mol. Struct. (Theochem)* **2003**, *636*, 203–214.
(31) Jezierska, A.; Panek, J.; Ryng, S.; Głowiak, T.; Koll, A. *J. Mol. Model.* **2003**, *9*, 159–163.
(32) Robertson, E. G. *J. Mol. Spectrosc.* **2005**, *231*, 50–56.
(33) Palmer, M. H.; Larsen, R. W.; Hegelund, F. *J. Mol. Spectrosc.* **2008**, *252*, 60–71.
(34) Pace, A.; Pierro, P.; Buscemi, S.; Vivon, N.; Barone, G. *J. Org. Chem.* **2009**, *74*, 351–358.
(35) Lifshitz, A.; Wohlfeilert, D. *J. Phys. Chem.* **1992**, *96*, 4505–4515.
(36) Higgins, J.; Zhou, X.; Liu, R. *J. Phys. Chem. A* **1997**, *101*, 7231–7235.
(37) Pérez, J. D.; Yranzo, G. I.; Wunderlin, D. A. *J. Org. Chem.* **1982**, *47*, 982–984.
(38) Nishiwaki, T.; Saito, T.; Onomura, S.; Kondo, K. *J. Chem. Soc. C* **1971**, 2644–2647.
(39) Pérez, J. D.; Wunderlin, D. A. *J. Org. Chem.* **1987**, *52*, 3637–3640.
(40) Padwa, A.; Chen, E.; Ku, A. *J. Am. Chem. Soc.* **1975**, *97*, 6484–6491.
(41) Singh, B.; Ullman, E. F. *J. Am. Chem. Soc.* **1967**, *89*, 6911–6916.
(42) Darlage, L. J.; Kinstle, T. H.; McIntosh, C. L. *J. Org. Chem.* **1971**, *36*, 1088–1093.
(43) Sauers, R. R.; Hadel, L. M.; Scimone, A. A.; Stevenson, T. A. *J. Org. Chem.* **1990**, *55*, 4011–4019.
(44) Ferris, J. P.; Trimmer, R. W. *J. Org. Chem.* **1976**, *42*, 13–19.
(45) Tanaka, H.; Matsushita, T.; Osamura, Y.; Nishimoto, K. *Int. J. Quantum Chem.* **1980**, *18*, 463–468.
(46) De Munno, A.; Bertini, V.; Luchesini, F. *J. Chem. Soc., Perkin Trans. 2* **1977**, 1121–1124.
(47) Lee, C. K. Y.; Easton, C. J.; Gebara-Coghlan, M.; Radom, L.; Scott, A. P.; Simpson, G. W.; Wills, A. C. *J. Chem. Soc., Perkin Trans. 2* **2002**, 2031–2038.
(48) Pavlik, J. W.; St. Martin, H.; Lambert, K. A.; Lowell, J. A.; Tsefrikas, V. M.; Eddins, C. K.; Kebede, N. *J. Heterocycl. Chem.* **2005**, *42*, 273–281.
(49) Lopes, S.; Nunes, C. M.; Fausto, R.; Pinho e Melo, T. M. V. D. *J. Mol. Struct.* **2009**, *919*, 47–53.
(50) Lopes, S.; Nunes, C. M.; Gómez-Zavaglia, A.; Pinho e Melo, T. M. V. D.; Fausto, R. *J. Phys. Chem. A* **2010**, *114*, 9074–9082.
(51) Frisch, M. J.; Trucks, G. W.; Schlegel, H. B.; Scuseria, G. E.; Robb, M. A.; Cheeseman, J. R.; Montgomery, J. A., Jr.; Vreven, T.; Kudin, K. N.; Burant, J. C.; Millam, J. M.; Iyengar, S. S.; Tomasi, J.;

Barone, V.; Mennucci, B.; Cossi, M.; Scalmani, G.; Rega, N.; Petersson, G. A.; Nakatsuji, H.; Hada, M.; Ehara, M.; Toyota, K.; Fukuda, R.; Hasegawa, J.; Ishida, M.; Nakajima, T.; Honda, Y.; Kitao, O.; Nakai, H.; Klene, M.; Li,X.; Knox, J. E.; Hratchian, H. P.; Cross, J. B.; Bakken, V.; Adamo, C.; Jaramillo, J.; Gomperts, R.; Stratmann, R. E.; Yazyev, O.; Austin, A. J.; Cammi, R.; Pomelli, C.; Ochterski, J. W.; Ayala, P. Y.; Morokuma, K.; Voth, G. A.; Salvador, P.; Dannenberg, J. J.; Zakrzewski, V. G.; Dapprich, S.; Daniels, A. D.; Strain, M. C.; Farkas, O.; Malick, D. K.; Rabuck, A. D.; Raghavachari, K.; Foresman, J. B.; Ortiz, J. V.; Cui, Q.; Baboul, A. G.; Clifford, S.; Cioslowski, J.; Stefanov, B. B.; Liu, G.; Liashenko, A.; Piskorz, P.; Komaromi, I.; Martin, R. L.; Fox, D. J.; Keith, T.; Al-Laham, M. A.; Peng, C. Y.; Nanayakkara, A.; Challacombe, M.; Gill, P. M. W.; Johnson, B.; Chen, W.; Wong, M. W.; Gonzalez, C.; Pople, J. A. *Gaussian 03*, revision C.02; Gaussian, Inc.: Wallingford, CT, 2004.

(52) Frisch, M.; Head-Gordon, M.; Pople, J. A. *Chem. Phys. Lett.* **1990**, *166*, 281–289.

(53) Becke, A. D. *Phys. Rev. A* **1988**, *38*, 3098–3100.

(54) Lee, C. T.; Yang, W. T.; Parr, R. G. *Phys. Rev. B* **1988**, *37*, 785–789.

(55) Császár, P.; Pulay, P. *J. Mol. Struct.* **1984**, *114*, 31–34.

(56) Farkas, Ö.; Schlegel, H. B. *J. Chem. Phys.* **1999**, *111*, 10806–10814.

(57) Peng, C.; Schlegel, H. B. *Isr. J. Chem.* **1994**, *33*, 449–454.

(58) Schachtschneider, J. H.; Mortimer, F. S. Vibrational Analysis of Polyatomic Molecules. VI. FORTRAN IV Programs for Solving the Vibrational Secular Equation and for the Least-Squares Refinement of Force Constants, Report No. 31450; Structural Interpretation of Spectra, Technical Report No. 57-650; Shell Development Co.: Emeryville, CA, 1969.

(59) Pulay, P.; Fogarasi, G.; Pang, F.; Boggs, J. E. *J. Am. Chem. Soc.* **1979**, *110*, 2550–2560.

(60) Kulbida, A.; Ramos, M. N.; Räsänen, M.; Nieminen, J.; Schrems, O.; Fausto, R. *J. Chem. Soc., Faraday Trans.* **1995**, *91*, 1571–1585.

(61) Reva, I. D.; Stepanian, S. G.; Adamowicz, L.; Fausto, R. *J. Phys. Chem. A* **2001**, *105*, 4773–4780.

(62) Wiberg, K. B. K. E.; Laidig, K. E. *J. Am. Chem. Soc.* **1987**, *109*, 5935–5943.

(63) Fausto, R.; Teixeira-Dias, J. J. C. *J. Mol. Struct.* **1986**, *144*, 215–223.

(64) Fausto, R.; Teixeira-Dias, J. J. C. *J. Mol. Struct.* **1987**, *150*, 381–389.

(65) Fausto, R.; Teixeira-Dias, J. J. C. *J. Mol. Struct. (Theochem.)* **1993**, *282*, 123–129.

(66) Li, G.; Kakarla, R.; Gerritz, S. W. *Tetrahedron. Lett.* **2007**, *48*, 4595–4599.

(67) Cioslowski, J. *J. Am. Chem. Soc.* **1989**, *111*, 8333–8336.

(68) Barnes, A. J. *J. Mol. Struct.* **1984**, *113*, 161–174.

(69) Reva, I. D.; Stepanian, S. G.; Adamowicz, L.; Fausto, R. *Chem. Phys. Lett.* **2003**, *374*, 631–638.

(70) Gómez-Zavaglia, A.; Fausto, R. *J. Mol. Struct.* **2004**, *689*, 199–212.

(71) Gómez-Zavaglia, A.; Kaczor, A.; Cardoso, A. L.; Pinho e Melo, T. M. V. D.; Fausto, R. *J. Phys. Chem. A* **2006**, *110*, 8081–8092.

(72) Borba, A.; Gómez-Zavaglia, A.; Simões, P. N. N. L.; Fausto, R. *J. Phys. Chem. A* **2005**, *109*, 3578–3586.

(73) Kaczor, A.; Gómez-Zavaglia, A.; Cardoso, A. L.; Pinho e Melo, T. M. V. D.; Fausto, R. *J. Phys. Chem. A* **2006**, *110*, 10742–10749.

(74) Fonseca, S. M.; Burrows, H. D.; Nunes, C. M.; Pinho e Melo, T. M. V. D. *Chem. Phys. Lett.* **2009**, *474*, 84–87.

(75) Sauers, R. R.; Van Arnum, S. D. *Tetrahedron Lett.* **1987**, *28*, 5797–5800.

(76) Tanaka, H.; Osamura, Y.; Matsushita, T; Nishimoto, K. *Bull. Chem. Soc. Jpn.* **1981**, *54*, 1293–1298.

(77) Orton, E.; Collins, S. T.; Pimentel, G. *J. Phys. Chem.* **1986**, *90*, 6139–6143.

(78) Inui, H.; Murata, S. *J. Am. Chem. Soc.* **2005**, *127*, 2628–2636.

(79) Kurtz, D. W.; Shechter, H. *Chem. Commun.* **1966**, *19*, 689–690.

(80) Yranzo, G. I.; Elguero, J. E.; Flammang, R.; Wentrup, C. *Eur. J. Org. Chem.* **2001**, 2209–2220.

(81) Charles, S. W.; Lee, K. O. *Trans. Faraday Soc.* **1965**, *61*, 614–619.

(82) Abe, H.; Yamada, K. M. T. *Struct. Chem.* **2003**, *14*, 211–215.